Available online at www.sciencedirect.com

ScienceDirect

International Journal of Solids and Structures 44 (2007) 587–602

INTERNATIONAL JOURNAL OF SOLIDS and STRUCTURES

www.elsevier.com/locate/ijsolstr

Smart damping of laminated thin cylindrical panels using piezoelectric fiber reinforced composites

M.C. Ray

Department of Mechanical Engineering, Indian Institute of Technology, Kharagpur 721302, West Bengal, India

Received 6 October 2005; received in revised form 12 April 2006
Available online 7 May 2006

Abstract

In this paper performance of a new piezoelectric fiber reinforced composite (PFRC) material has been investigated for active constrained layer damping (ACLD) of laminated thin simply supported composite cylindrical panels. The constraining layer of the ACLD treatment has been considered to be made of this PFRC material. A finite element model of smart composite panels integrated with the patches of such ACLD treatment has been developed to demonstrate the performance of these patches on enhancing the damping characteristics of thin cross-ply and angle-ply laminated composite cylindrical panels. Particular emphasis has been placed on studying the effect of variation of the piezoelectric fiber orientation in the constraining PFRC layer and the shallowness angle of the panels on the control authority of the patches.

Keywords: Smart structures; Piezoelectric composites; Constrained layer damping; Active control

1. Introduction

Piezoelectric sensors and/or actuators are being extensively used for active vibration control of light weight smart structures during the past one and half decade (Bailey and Hubbard, 1985; Crawley and Luis, 1987; Baz and Poh, 1988; Tzou and Tseng, 1990; Lee et al., 1991; Hanagud et al., 1992; Devasia et al., 1993; Gu et al., 1994; Zhou et al., 1995; Baz and Poh, 1996; Agarwal and Treanor, 1999; Stöbener and Gaul, 2000; Dong and Tong, 2001; Peng et al., 2005). The direct and converse piezoelectric effects inherently present in these materials are utilized for using these materials as distributed sensors and actuators, respectively. Customarily, the flexible structures integrated with a layer/patch of these materials acting as distributed sensors and/or actuators are called as ''Smart Structures''. One of the drawbacks of the existing monolithic piezoelectric materials is that the magnitudes of the piezoelectric coefficients of these materials are very low. Since the performance of smart structures depends on the magnitude of these piezoelectric stress/strain coefficients, large control voltage is necessary for achieving significant active damping of smart structures if the piezoelectric actuators are directly bonded to the host structures. For better utilization of these low control authority piezoelectric

E-mail address: mcray@mech.iitkgp.ernet.in

0020-7683/$ - see front matter
doi:10.1016/j.ijsolstr.2006.05.005

materials, concept of active constrained layer damping (ACLD) treatment was emerged. If the constraining layer of the conventional passive constrained layer damping (PCLD) treatment (Plunkett and Lee, 1970) is replaced by a layer of piezoelectric material, the resulting treatment has been named as active constrained layer damping (ACLD) treatment (Baz and Ro, 1995; Azvine et al., 1995). When the ACLD treatment is integrated with a host structure (substrate) and the constraining layer of the treatment is augmented with an appropriate control means, the transverse shear deformation of the viscoelastic constrained layer can be increased over its passive counterpart and the vibration of the host structure can be substantially damped out leading to the active or smart constrained layer damping of this structure (Baz and Ro, 1995). The flexural vibration control by the constrained layer damping treatment is attributed to the dissipation of energy in the constrained viscoelastic core undergoing transverse shear deformation. Since the task of deforming the viscoelastic layer is easier than the task of deforming the host structure, the piezoelectric materials perform much better to attenuate the vibration of smart structures when they are used as active constraining layer of the ACLD treatment than when they are used alone as the distributed actuators. Also, as the constraining layer of the ACLD treatment can become passive and active under operation, the ACLD treatment provides the attributes of both passive and active damping. Hence, since its inception ACLD treatment has gained tremendous importance for efficient and reliable active control of flexible structures (Baz and Ro, 1996; Shen, 1996; Kapadia and Kawiecki, 1997; Badre-Alam et al., 1999; Sung and Kam, 2000; Ray et al., 2001; Chantalakhana and Stanway, 2001; Ro and Baz, 2002; Liu and Wang, 2002; Sun and Tong, 2003; Ray and Reddy, 2004; Yau and Fung, 2005).

Performance of smart structures can further be improved if the constraining layer of the ACLD treatment is made of the piezoelectric materials with improved piezoelectric coefficients. Recently, Mallik and Ray (2003) and Ray and Mallik (2004) investigated the effective elastic and piezoelectric properties of unidirectional piezoelectric fiber reinforced composite (PFRC) materials. The investigations revealed that the effective piezoelectric co-efficient denoted by e_{31} of these PFRC materials which quantifies the induced normal stress in the fiber direction due to the applied electric field in the direction transverse to the fiber direction becomes significantly larger than the corresponding co-efficient of the piezoelectric material of the fibers within the useful range (0.4–0.8) of fiber volume fraction. Since the in-plane actuation of a lamina of this PFRC material is utilized for structural vibration control, the effective piezoelectric coefficient, e_{31} of this PFRC material is mainly responsible for active control of flexural vibrations of smart structures. Ray and Mallik (2004,a, 2005b) and Ray and Reddy (2005) also investigated the performance of this PFRC material as the material for distributed actuators of smart laminated composite beams, plates and circular closed cylindrical shells. Laminated thin cylindrical composite panels (shallow shells) are an important class of structures being used for manufacturing various parts of commercial aircrafts, automobiles and the like. Unlike the complete circular cylindrical shell which involves only two curved edge boundaries, a circular cylindrical panel has two curved edge boundaries and two straight edge boundaries. Hence, for a given plan-form the dynamical characteristics of cylindrical panels (shallow shells) are different from those of the closed circular cylindrical shells. Thus separate attention is necessary to investigate the active control of cylindrical panels even though the author has already studied the active control of closed circular cylindrical shells (Ray and Reddy, 2005). However, to the author's best knowledge, active constrained layer damping of laminated cylindrical composite panels using piezoelectric fiber reinforced composite (PFRC) materials has not yet been addressed.

In this paper, performance of the active constraining layer of the ACLD treatment in which the active constraining layer is made of the PFRC material as described above has been investigated for active control of laminated thin cylindrical composite panels. A simple finite element model has been developed considering the equivalent single layer first order shear deformation theories. Emphasis is placed on investigating the effect of fiber orientation in the constraining PFRC layer on the active damping of thin antisymmetric cross-ply and angle-ply panels using this finite element model. Also, the effect of variation of the shallowness angle of the panel on the performance of the constraining PFRC layer of the ACLD treatment has been investigated.

2. Finite element model

Fig. 1 shows a laminated cylindrical composite panel made of N number of orthotropic layers. The length, circumferential width, thickness, average radius and shallowness angle of the panel are denoted by a, s, h, R

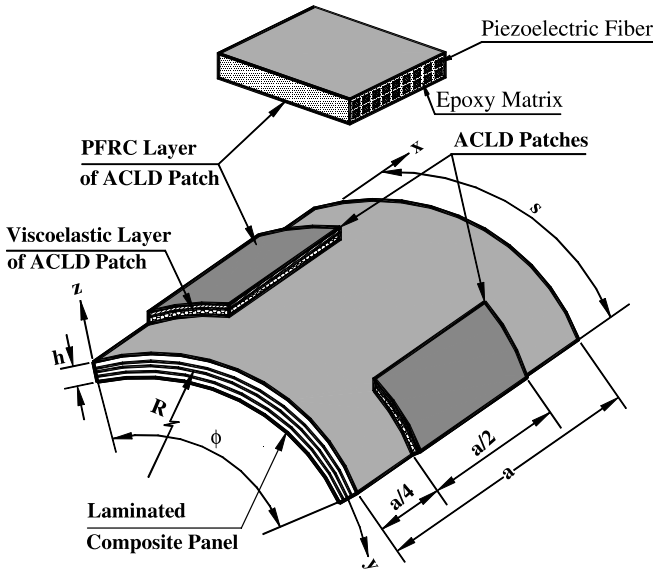

Fig. 1. Schematic representation of laminated composite panel integrated with the patches of ACLD treatment.

and ϕ, respectively. The top surface of the panel is integrated with the rectangular patches of ACLD treatment. The constraining layer of the ACLD treatment is made of the piezoelectric fiber reinforced composite (PFRC) material in which the fibers are unidirectionally aligned and parallel to the plane of the panel and its constructional feature is also schematically demonstrated in Fig. 1. The thickness of the PFRC layer is h_p and that of the viscoelastic constrained layer of the ACLD treatment is h_v. The mid-plane of the substrate panel is considered as the reference plane. The origin of the curvilinear laminate coordinate system (x, y, z) is located at one corner of the reference plane such that the lines $x = 0$ and a and $y = 0$ and s represent the boundaries of the panels. The thickness coordinates (z) of the top and bottom surfaces of any (kth) layer $(k = 1, 2, 3, \ldots, N + 2)$ of the overall laminated panel are represented by h_{k+1} and h_k, respectively. The fiber orientation in any layer of the substrate panel with respect to the laminate coordinate system is denoted by θ while that in the active constraining layer of the PFRC material is denoted by ψ. First order shear deformation theories (FSDT) are used for modeling the kinematics of deformation of the overall panel integrated with the patches of ACLD treatment. Fig. 2 describes a schematic representation of the kinematics of deformation based on these theories. As shown in this figure, u_0 and v_0 are the generalized translational displacements of a reference point (x, y) on the mid-plane $(z = 0)$ of the substrate panel along x- and y-axes, respectively; θ_x, ϕ_x and γ_x are the generalized rotations of the normal to the middle planes of the substrate, viscoelastic layer and the PFRC layer, respectively about y-axis while the generalized rotations of these normal about x-axis are denoted respectively by θ_y, ϕ_y and γ_y. According to the kinematics of deformation shown in Fig. 2, the

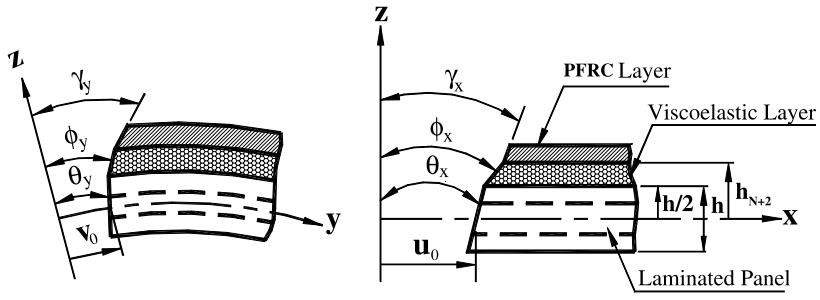

Fig. 2. Kinematics of deformation.

displacements u, v and w at any point lying in any layer of the overall panel along x-, y- and z-directions, respectively can be expressed as

$$\{d\} = \{d_t\} + [Z]\{d_r\} \tag{1}$$

where,

$$\{d\} = [\,u \quad v \quad w\,]^T, \quad \{d_t\} = [\,u_0 \quad v_0 \quad w\,]^T, \quad \{d_r\} = [\,\theta_x \quad \theta_y \quad \phi_x \quad \phi_y \quad \gamma_x \quad \gamma_y\,]^T,$$
$$[Z] = \begin{bmatrix} \lambda_1(z) & 0 & \lambda_2(z) & 0 & \lambda_3(z) & 0 \\ 0 & \lambda_1(z) & 0 & \lambda_2(z) & 0 & \lambda_3(z) \\ 0 & 0 & 0 & 0 & 0 & 0 \end{bmatrix}, \quad \lambda_1(z) = z - \langle z - h/2\rangle,$$
$$\times\, \lambda_2(z) = \langle z - h/2\rangle - \langle z - h_{N+2}\rangle \quad \text{and} \quad \lambda_3(z) = \langle z - h_{N+2}\rangle \tag{2}$$

Note that the appropriate singularity functions denoted by the bracketed functions $\langle\cdot\rangle$ are used to represent the three first order shear deformation theories respectively for modeling the substrate panel, the viscoelastic layer and the PFRC layer while maintaining the continuity conditions. In order to implement the selective integration rule necessary for avoiding the shear locking problem in thin structures, the state of strains at any point in the overall panel is divided into the state of in-plane strains $\{\epsilon_b\}$ and the state of transverse shear strains $\{\epsilon_s\}$ as follows:

$$\{\epsilon_b\} = [\,\epsilon_x \quad \epsilon_y \quad \epsilon_{xy}\,]^T \quad \text{and} \quad \{\epsilon_s\} = [\,\epsilon_{xz} \quad \epsilon_{yz}\,]^T \tag{3}$$

in which ϵ_x, ϵ_y are the normal strains along x- and y-directions, respectively; ϵ_{xy} is the in-plane shear strain; ϵ_{xz} and ϵ_{yz} are the transverse shear strains. Using the displacement fields, given by (1) and (2), the linear strain displacement relations for circular cylindrical panels (Soldatos, 1984) and Eq. (3), the state of strains at any point in the overall panel can be written in terms of the generalized translational $\{d_t\}$ and rotational displacements $\{d_r\}$ as follows:

$$\{\epsilon_b\} = [L_{tb}]\{d_t\} + [Z_1][L_{rb}]\{d_r\} \quad \text{and} \quad \{\epsilon_s\} = [L_{ts}]\{d_t\} + [Z_2]\{d_r\} \tag{4}$$

in which the matrices $[Z_1]$ and $[Z_2]$ and the different operator matrices are defined as

$$[Z_1] = [\,\{\lambda_1(z)\}I \quad \{\lambda_2(z)\}I \quad \lambda_3(z)I\,]$$
$$[Z_2] = \begin{bmatrix} \lambda_4(z) & 0 & \lambda_5(z) & 0 & \lambda_6(z) & 0 \\ 0 & \lambda_4(z) - \dfrac{1}{R}\lambda_1(z) & 0 & \lambda_5(z) - \dfrac{1}{R}\lambda_2(z) & 0 & \lambda_6(z) - \dfrac{1}{R}\lambda_3(z) \end{bmatrix}$$
$$\lambda_4(z) = 1 - \langle z - h/2\rangle^0, \quad \lambda_5(z) = \langle z - h/2\rangle^0 - \langle z - h_{N+2}\rangle^0, \quad \lambda_6(z) = \langle z - h_{N+2}\rangle^0$$
$$[L_{tb}] = [\,L_1 \quad L_f 2\,], \quad L_1 = \begin{bmatrix} \dfrac{\partial}{\partial x} & 0 \\ 0 & \dfrac{\partial}{\partial y} \\ \dfrac{\partial}{\partial y} & \dfrac{\partial}{\partial x} \end{bmatrix}, \quad L_2 = \begin{bmatrix} 0 & \dfrac{1}{R} & 0 \end{bmatrix}^T \tag{5}$$
$$[L_{rb}] = \begin{bmatrix} L_1 & \widetilde{O} & \widetilde{O} \\ \widetilde{O} & L_1 & \widetilde{O} \\ \widetilde{O} & \widetilde{O} & L_1 \end{bmatrix} \quad \text{and} \quad [L_{ts}] = \begin{bmatrix} 0 & 0 & \dfrac{\partial}{\partial x} \\ 0 & -\dfrac{1}{R} & \dfrac{\partial}{\partial y} \end{bmatrix}$$

wherein, I and $\widetilde{O}$ appearing in the matrices $[Z_1]$ and $[L_{rb}]$ are a (3×3) identity matrix and a (3×2) null matrix, respectively. Corresponding to the description of the state of strains given by Eq. (3), the state of in-plane stresses and the state of transverse shear stresses at any point in the overall panel can be expressed as

$$\{\sigma_b\} = [\,\sigma_x \quad \sigma_y \quad \sigma_{xy}\,]^T \quad \text{and} \quad \{\sigma_s\} = [\,\sigma_{xz} \quad \sigma_{yz}\,]^T \tag{6}$$

where σ_x, σ_y are the normal stresses along x- and y-directions, respectively; σ_{xy} is the in-plane shear stress; σ_{xz} and σ_{yz} are the transverse shear stresses.

The constitutive relations for the material of any (kth) orthotropic layer of the host panel are given by

$$\{\sigma_b^k\} = [\overline{C}_b^k]\{\epsilon_b^k\} \quad \text{and} \quad \{\sigma_s^k\} = [\overline{C}_s^k]\{\epsilon_s^k\}, \quad k = 1, 2, \ldots, N \tag{7}$$

The constraining PFRC layer will be subjected to the applied electric field (E_z) acting across its thickness (i.e. along the z-direction) only. Thus the constitutive relations for the material of the PFRC layer can be expressed as (Mallik and Ray, 2003)

$$\begin{aligned} &\{\sigma_b^k\} = [\overline{C}_b^k]\{\epsilon_b^k\} - \{\bar{e}_b\}E_z \quad \text{and} \quad \{\sigma_s^k\} = [\overline{C}_s^k]\{\epsilon_s^k\}, \quad k = N+2 \\ &D_z = \{\bar{e}_b^k\}^T\{\epsilon_b^k\} + \bar{\varepsilon}_{33}E_z, \quad k = N+2 \end{aligned} \tag{8}$$

in which D_z is the electric field in the z-direction and $\bar{\varepsilon}_{33}$ is the transformed dielectric constant. The transformed elastic coefficient matrices $[\overline{C}_b^k]$, $[\overline{C}_s^k]$ and the transformed piezoelectric coefficient matrix $\{\bar{e}_b\}$ appearing in Eqs. (7) and (8), referred to the laminate coordinate (x, y, z) system are given by

$$[\overline{C}_b^k] = \begin{bmatrix} \overline{C}_{11}^k & \overline{C}_{12}^k & \overline{C}_{16}^k \\ \overline{C}_{12}^k & \overline{C}_{22}^k & \overline{C}_{26}^k \\ \overline{C}_{16}^k & \overline{C}_{26}^k & \overline{C}_{66}^k \end{bmatrix}, \quad [\overline{C}_s^k] = \begin{bmatrix} \overline{C}_{55}^k & \overline{C}_{45}^k \\ \overline{C}_{45}^k & \overline{C}_{44}^k \end{bmatrix} \quad \text{and} \quad \{\bar{e}_b\} = \begin{Bmatrix} \bar{e}_{31} \\ \bar{e}_{32} \\ \bar{e}_{36} \end{Bmatrix} \tag{9}$$

The viscoelastic material of the constraining layer considered in this study is assumed to be linearly viscoelastic and isotropic and is considered to be modeled by the commonly used complex modulus approach which is a frequency domain based model. When the complex modulus approach is employed, the constitutive relation for the viscoelastic material can also be represented by Eq. (7) with $k = N+1$ while the shear modulus G and Young's modulus E of the viscoelastic material are given by Shen (1996), Kapadia and Kawiecki (1997), Badre-Alam et al. (1999), Sung and Kam (2000), Ray et al. (2001), Chantalakhana and Stanway (2001), Ro and Baz (2002) and Liu and Wang (2002)

$$G = G'(1 + i\eta) \quad \text{and} \quad E = 2G(1 + \upsilon) \tag{10}$$

in which G' is the storage modulus, υ is the Poisson's ratio and η is the loss factor at a particular operating temperature and frequency. Using (10), the elastic coefficients of the viscoelastic material can be computed and the resulting elastic coefficient matrix $[\overline{C}^{N+1}]$ turns out to be a complex matrix.

The energy functional T_p of the panel integrated with the patches of ACLD treatment describing the total energy comprising of the strain energy, electrical energy and the work done by the external load can be written as (Ray and Mallik, 2005b)

$$T_p = \frac{1}{2}\left[\sum_{k=1}^{N+2}\int_\Omega \left(\{\epsilon_b^k\}^T\{\sigma_b^k\} + \{\epsilon_s^k\}^T\{\sigma_s^k\}\right)d\Omega - \int_\Omega E_z D_z\, d\Omega\right] - \int_A \{d\}^T\{f\}\, dA \tag{11}$$

while the total kinetic energy T_k of the overall panel can be expressed as

$$T_k = \frac{1}{2}\left[\sum_{k=1}^{N+2}\int_\Omega \rho^k(\dot{u}^2 + \dot{v}^2 + \dot{w}^2)d\Omega\right] \tag{12}$$

in which, $\{f\}$ is the externally applied surface traction vector acting over a surface area A, Ω represents the volume of the kth layer in concern and ρ^k is the mass density of this layer.

The overall panel has been discretized by eight noded isoparametric quadrilateral elements. Following Eq. (2), the generalized displacement vectors for the ith ($i = 1, 2, 3, \ldots, 8$) node of an element can be represented as

$$\{d_{ti}\} = [\,u_{0i} \quad v_{0i} \quad w_i\,]^T \quad \text{and} \quad \{d_{ri}\} = [\,\theta_{xi} \quad \theta_{yi} \quad \phi_{xi} \quad \phi_{yi} \quad \gamma_{xi} \quad \gamma_{yi}\,]^T \tag{13}$$

Thus the generalized displacement vectors at any point within the element can be written as

$$\{d_t\} = [N_t]\{d_t^e\} \quad \text{and} \quad \{d_r\} = [N_r]\{d_r^e\} \tag{14}$$

wherein, $\{d_t^e\}$ is the nodal generalized translational displacement vector, $\{d_r^e\}$ the nodal generalized rotational displacement vector, $[N_t]$ and $[N_r]$ the shape function matrices. The detail form of these matrices are given by

$$\begin{aligned}&\{d_t^e\} = \left[\{d_{t1}\}^T \quad \{d_{t2}\}^T \quad \cdots \quad \{d_{t8}\}^T\right]^T, \quad \{d_r^e\} = \left[\{d_{r1}\}^T \quad \{d_{r2}\}^T \quad \cdots \quad \{d_{r8}\}^T\right]^T,\\ &[N_t] = [N_{t1} \quad N_{t2} \quad \cdots \quad N_{t8}], \quad [N_r] = [N_{r1} \quad N_{r2} \quad \cdots \quad N_{r8}], \quad N_{ti} = n_i I, \quad N_{ri} = n_i I_2\end{aligned} \tag{15}$$

in which I_2 is a (6×6) identity matrix and n_i is the shape function of natural coordinates associated with the ith node of the element. On substitution of Eq. (14) into Eq. (4), the strain vectors at any point within the element can be expressed in terms of the nodal generalized displacements as follows:

$$\{\epsilon_b\} = [B_{tb}]\{d_t^e\} + [Z_1][B_{rb}]\{d_r^e\} \quad \text{and} \quad \{\epsilon_s\} = [B_{ts}]\{d_t^e\} + [B_{rs}]\{d_r^e\} \tag{16}$$

in which the nodal strain–displacement matrices are given by

$$[B_{tb}] = [L_{tb}][N_t], [B_{rb}] = [L_{rb}][N_r], [B_{ts}] = [L_{ts}][N_t] \quad \text{and} \quad [B_{rs}] = [N_r] \tag{17}$$

Substituting Eqs. (7) and (8) into Eq. (13) and then using Eq. (16), the energy functional T_p^e of a typical element integrated with the ACLD treatment can be derived as

$$\begin{aligned}T_p^e = \frac{1}{2}\Big[&\{d_t^e\}^T[K_{tt}^e]\{d_t^e\} + \{d_t^e\}^T[K_{tr}^e]\{d_r^e\} + \{d_r^e\}^T[K_{tr}^e]^T\{d_t^e\} + \{d_r^e\}^T[K_{rr}^e]\{d_r^e\} - 2\{d_t^e\}^T\{f_{tp}^e\}V\\ &- 2\{d_r^e\}^T\{f_{rp}^e\}V - 2\{d_t^e\}^T\{F^e\} - \bar{\varepsilon}_{33}\overline{E}^2V^2\Big]\end{aligned} \tag{18}$$

in which $\overline{E} = -1/h_p$ and V is the potential difference across the thickness of the PFRC layer. The elemental stiffness matrices $[K_t^e]$, $[K_{tr}^e]$, $[K_{rr}^e]$; the elemental electro-elastic coupling vectors $\{F_{tp}^e\}$, $\{F_{rp}^e\}$ and the elemental load vector $\{F^e\}$ appearing in Eq. (18) are given by

$$\begin{aligned}[K_{tt}^e] &= \int_0^{b_e}\int_0^{a_e}\Big([B_{tb}]^T[D_{tb}][B_{tb}] + [B_{ts}]^T[D_{ts}][B_{ts}]\Big)\mathrm{d}x\,\mathrm{d}y,\\ [K_{tr}^e] &= \int_0^{b_e}\int_0^{a_e}\Big([B_{tb}]^T[D_{trb}][B_{rb}] + [B_{ts}]^T[D_{trs}][B_{rs}]\Big)\mathrm{d}x\,\mathrm{d}y,\\ [K_{rr}^e] &= \int_0^{b_e}\int_0^{a_e}\Big([B_{rb}]^T[D_{rrb}][B_{rb}] + [B_{rs}]^T[D_{rrs}][B_{rs}]\Big)\mathrm{d}x\,\mathrm{d}y\\ \{f_{tp}^e\} &= \int_0^{b_e}\int_0^{a_e}[B_{tb}]^T\{F_{tb}\}_p\mathrm{d}x\,\mathrm{d}y, \quad \{f_{rp}^e\} = \int_0^{b_e}\int_0^{a_e}[B_{rb}]^T\{F_{rb}\}_p\mathrm{d}x\,\mathrm{d}y \quad \text{and}\\ \{F^e\} &= \int_0^{b_e}\int_0^{a_e}[N_t]^T\{f\}\mathrm{d}x\,\mathrm{d}y.\end{aligned}$$

wherein, a_e and b_e are the length and circumferential width of the element in consideration and the various rigidity matrices originated in the above elemental matrices are given by

$$\begin{aligned}&[D_{tb}] = \sum_{k=1}^{N+2}\int_{h_k}^{h_{k+1}}[\overline{C}_b^k]\mathrm{d}z, \quad [D_{trb}] = \sum_{k=1}^{N+2}\int_{h_k}^{h_{k+1}}[\overline{C}_b^k][Z_1]\mathrm{d}z, \quad [D_{rrb}] = \sum_{k=1}^{N+2}\int_{h_k}^{h_{k+1}}[Z_1]^T[\overline{C}_b^k][Z_1]\mathrm{d}z\\ &[D_{trs}] = \sum_{k=1}^{N+2}\int_{h_k}^{h_{k+1}}[\overline{C}_s^k][Z_2]\mathrm{d}z, \quad [D_{rrs}] = \sum_{k=1}^{N+2}\int_{h_k}^{h_{k+1}}[Z_2]^T[\overline{C}_s^k][Z_2]\mathrm{d}z\\ &\{F_{tb}\}_p = \int_{h_{N+2}}^{h_{N+3}}\{\bar{e}_b\}\overline{E}\,\mathrm{d}z \quad \text{and} \quad \{F_{rb}\}_p = \int_{h_{N+2}}^{h_{N+3}}[Z_1]^T\{\bar{e}\}\overline{E}\,\mathrm{d}z\end{aligned}$$

Since the viscoelastic material is modeled by the complex modulus approach, the elemental stiffness matrices derived as above are complex for an element augmented with the ACLD treatment. Note that the derivation and the expressions of the elemental matrices appear to be much simpler than those presented in Ray and Reddy (2005) even though the same displacement theories are used. This is because of the fact that the same expressions are used to represent the strain-nodal displacement relations given by Eq. (16) and the rigidity matrices for the host panel, viscoelastic layer and the piezoelectric layer through the use of singularity

functions. Substituting (14) into Eq. (12) and neglecting the rotary inertia of the overall panel as the host panel is very thin, the expression for kinetic energy T_k^e of the element can be obtained as

$$T_k^e = \frac{1}{2}\{\dot{d}_t^e\}^T[M^e]\{\dot{d}_t^e\} \tag{19}$$

in which the elemental mass matrix $[M^e]$ is given by

$$[M^e] = \int_0^{a_e}\int_0^{b_e}\left(\sum_{k=1}^{N}\rho^k(h_{k+1}-h_k) + \rho^{N+1}h_v + \rho^{N+2}h_p\right)[N_t]^T[N_t]\mathrm{d}x\,\mathrm{d}y.$$

Using the principle of virtual work (Ro and Baz, 2002), one can derive the governing equations of an element as follows:

$$[M^e]\{\ddot{d}_t^e\} + [K_{tt}^e]\{d_t^e\} + [K_{tr}^e]\{d_r^e\} = \{f_{tp}^e\}V + \{F^e\} \tag{20}$$

$$[K_{tr}^e]^T\{d_t^e\} + [K_{rr}^e]\{d_r^e\} = \{f_{rp}^e\}V \tag{21}$$

It is to be noted now that in case of an element without integrated with the ACLD treatment, the electro-elastic coupling matrices $\{f_{tp}^e\}$, $\{f_{rp}^e\}$ turn out to be the null matrices and the other elemental stiffness matrices in Eqs. (20) and (21) become real.

The elemental equations of motion are assembled to form the global equations of motion in such a manner that each patch can be activated separately as follows:

$$[M]\{\ddot{X}\} + [K_{tt}]\{X\} + [K_{tr}]\{X_r\} = \sum_{j=1}^{m}\{F_{tp}^j\}V^j + \{F\} \tag{22}$$

$$[K_{tr}]^T\{X\} + [K_{rr}]\{X_r\} = \sum_{j=1}^{m}\{F_{rp}^j\}V^j \tag{23}$$

where $[M]$ is the global mass matrix; $[K_{tt}]$, $[K_{tr}]$, $[K_{rr}]$ are the global stiffness matrices; $\{X\}$ and $\{X_r\}$ are the global nodal translational and rotational degrees of freedom; $\{F_{tp}^j\}$ and $\{F_{rp}^j\}$ are the global electro-elastic coupling matrices corresponding to the jth patch, V^j is the voltage applied to this patch, m is the number of patches and $\{F\}$ is the global nodal force vector. After invoking the boundary conditions, the global rotational degrees of freedom can be eliminated to derive the global open loop equations of motion in terms of the global translational degrees of freedom only as follows:

$$[M]\{\ddot{X}\} + [K^*]\{X\} = \sum_{j=1}^{m}\{F_p^j\}V^j + \{F\} \tag{24}$$

in which $[K^*] = [K_{tt}] - [K_{tr}][K_{rr}]^{-1}[K_{tr}]^T$ and $\{F_p^j\} = \{F_{tp}^j\} - [K_{tr}][K_{rr}]^{-1}\{F_{rp}^j\}$.

3. Active and passive damping

In order to activate the patches of the ACLD treatment, a simple velocity feedback control law has been employed. According to this law, the control voltage for each patch is considered to be negatively proportional to the velocity of a point on the bottom of the host panel. Thus the control voltage supplied to each patch can be expressed in terms of the derivatives of the global nodal degrees of freedom as follows:

$$V^j = -K_d^j\dot{w} = -K_d^j[N^j]\{\dot{X}\} \tag{25}$$

in which K_d^j is the control gain for the jth patch and $[N^j]$ is a row vector defining the location of the concerned point for sensing the velocity signal that will be fed back to this patch. Finally, substituting Eq. (25) into Eq. (24), the equations of motion governing the closed loop dynamics of the substrate panels activated by the patches of ACLD treatments can be derived as follows:

$$[M]\{\ddot{X}\} + [C_d]\{\dot{X}\} + [K^*]\{X\} = \{F\} \tag{26}$$

It is obvious from Eq. (26) that the implementation of the control strategy yields the active damping matrix $[C_d]$ given by

$$[C_d] = \sum_{j=1}^{m} K_d^j \left\{ F_p^j \right\} [N^j] \tag{27}$$

Since the stiffness matrices for an element augmented with the ACLD treatment are complex, the global stiffness matrix $[K^*]$ becomes complex and its imaginary part is responsible for contribution to the dissipation of energy (Baz and Ro, 1996; Shen, 1996; Kapadia and Kawiecki, 1997; Badre-Alam et al., 1999; Sung and Kam, 2000; Ray et al., 2001; Chantalakhana and Stanway, 2001; Ro and Baz, 2002; Liu and Wang, 2002; Sun and Tong, 2003; Ray and Reddy, 2004; Yau and Fung, 2005). Hence, in the absence of applied control voltage the equations of motion given by Eq. (24) govern the passive (uncontrolled) constrained layer damping of the substrate panels (Baz and Ro, 1996; Shen, 1996; Kapadia and Kawiecki, 1997; Badre-Alam et al., 1999; Sung and Kam, 2000; Ray et al., 2001; Chantalakhana and Stanway, 2001; Ro and Baz, 2002; Liu and Wang, 2002; Sun and Tong, 2003; Ray and Reddy, 2004; Yau and Fung, 2005). In order to study the performance of the panels in frequency domain, it is considered that the panels are subjected to time-harmonic excitation force and the motion is harmonic. Thus it can be written that

$$\{X\} = \{\overline{X}\} e^{-i\omega t} \quad \text{and} \quad \{F\} = \{\overline{F}\} e^{-i\omega t} \tag{28}$$

where, $\{\overline{X}\}$ and $\{\overline{F}\}$ are the vectors of amplitudes of the nodal displacements and excitation forces and ω is the frequency of excitation. Substitution of Eq. (28) into Eq. (26) leads to the following algebraic equation:

$$\{\overline{X}\} = [K_{eq}]^{-1} \{\overline{F}\} \tag{29}$$

in which $[K_{eq}] = -\omega^2[M] - i\omega[C_d] + [K^*]$. Using Eq. (29), computation of $\{\overline{X}\}$ for any excitation frequency derives the frequency response functions of the panels coupled with the ACLD patches.

4. Numerical results

In this section, the numerical results are evaluated using the finite element model derived in the previous section. Both antisymmetric cross-ply and angle-ply thin circular cylindrical simply supported panels having the square plan form ($a \times a$) and integrated with two rectangular patches of ACLD treatment are considered as the numerical examples. The patches are placed on the outer surfaces of the panels as shown in Fig. 1. Unless otherwise mentioned, the length and width of the patches are assumed to be one fourth of the length and outer circumferential width of the panels, respectively and the piezoelectric fiber orientation in the constraining PFRC layer is 0°. The thicknesses of the PFRC layer, the viscoelastic layer and the laminated panels are considered as 150 μm, 50.8 μm and 3 mm, respectively. Also, unless otherwise mentioned, the values of the axial length (a) and the shallowness angle (ϕ) of the panels are considered as 0.5 m and 30°, respectively. The materials of the piezoelectric fiber and the matrix of the PFRC layer are considered as PZT5H and epoxy, respectively. Considering 40% fiber volume fraction, the following elastic and piezoelectric properties of the PFRC layer with respect to its material coordinate system are obtained from the existing micromechanics model (Mallik and Ray, 2003) and are used for evaluating the numerical results

$$C_{11} = 32.6 \text{ GPa}, \quad C_{12} = 4.3 \text{ GPa}, \quad C_{22} = 7.2 \text{ GPa}, \quad C_{44} = 1.05 \text{ GPa}, \quad C_{55} = C_{66} = 1.29 \text{ GPa},$$
$$e_{31} = -6.76 \text{ C/m}^2, \quad \rho = 3640 \text{ kg/m}^3$$

The material properties considered for the orthotropic layers of the substrate panels are considered as follows:

$$E_L = 172.9 \text{ GPa}, \quad E_L/E_T = 25, \quad G_{LT} = 0.5E_T, \quad G_{TT} = 0.2E_T, \quad \nu_{LT} = \nu_{TT} = 0.25, \quad \rho = 1600 \text{ kg/m}^3$$

in which the symbols have their usual meaning. The viscoelastic material used by Chantalakhana and Stanway (2001) is considered in this study to evaluate the numerical results. The loss factor of this viscoelastic material considered in this study remains invariant (Chantalakhana and Stanway, 2001) within a frequency range

(0–600 Hz) of interest and the values of the complex shear modulus, the Poisson's ratio and the density of this viscoelastic layer are $20(1+i)$MPa, 0.49 and 1140 kg/m^3, respectively (Chantalakhana and Stanway, 2001). The simply supported boundary conditions (Soldatos, 1984; Soldatos, 1983) at the edges of the overall panels considered for evaluating the numerical results are given by

$$v_0 = w = \theta_y = \phi_y = \gamma_y = 0 \quad \text{at } x = 0, a \quad \text{and} \quad u_0 = w = \theta_x = \phi_x = \gamma_x = 0 \quad \text{at } y = 0, s$$

In order to verify the validity of the present finite element model, the natural frequencies of the antisymmetric cross-ply and angle-ply panels integrated with the inactivated patches of negligible thickness are first computed and subsequently compared with the existing analytical results (Soldatos, 1984, 1983) of identical panels without integrated with the patches. Table 1 demonstrates this comparison of the fundamental natural frequencies of two layered antisymmetric cross-ply and angle-ply cylindrical panels. It may be observed from this Table that the results are in excellent agreement.

The open and closed loop behavior of the panels are studied by the frequency response functions evaluated at a point $(a/2, s/4, h/2)$ on the top surface of the panels. A time harmonic point force $(2N)$ is considered to act at a point $(a/4, s/4, h/2)$ to excite the first few modes of the panels. The control voltage supplied to each patch is negatively proportional to the velocity of the point located on the panel outer surface which corresponds to the midpoint of the free length of the patch. Fig. 3 illustrates the frequency response functions of a two layered antisymmetric cross-ply (0°/90°) panel and the variation of the required control voltage applied to each patch with the frequency of excitation has been shown in Fig. 4 when the value of control gain is 1200. Displayed in Fig. 3 are the responses of the panel when the patches are passive (uncontrolled) and active with different control gains. It is evident from these figures that the active patches significantly improve the damping characteristics of the panel for both the modes over the passive damping with very low control voltage (Fig. 4). As the

Table 1
Fundamental non-dimensional fundamental frequencies (ϖ) of cross-ply and angle-ply panels with negligible thickness of PFRC layer[a]

Panel type and Parameters	Source	ϖ
(90°/0°), $a/s = 1$, $s/R = 0.5$, $R/h = 40$	Present FEM	11.53
	Analytical (Soldatos, 1984)	11.65
(45°/−45°), $\phi = 20°$, $a/h = 20$	Present FEM	26.06
	Analytical (Soldatos, 1983)	26.166

[a] $\varpi = \omega_{\min} a^2 \sqrt{\rho/(E_T h)}$, $\omega_{\min}$ = fundamental frequency.

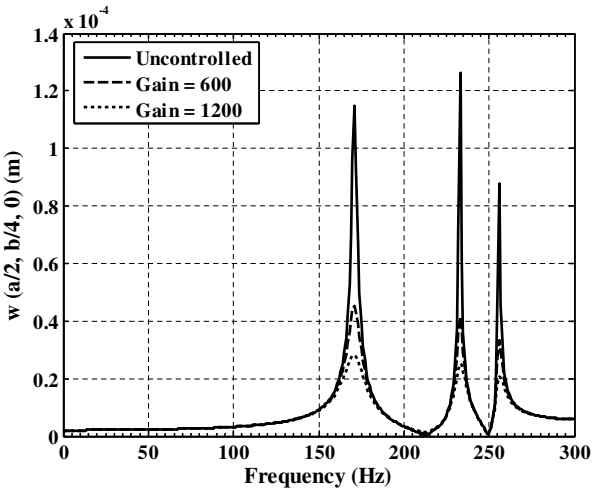

Fig. 3. Frequency response of an antisymmetric cross-ply (90°/0°) panel ($\phi = 30°$).

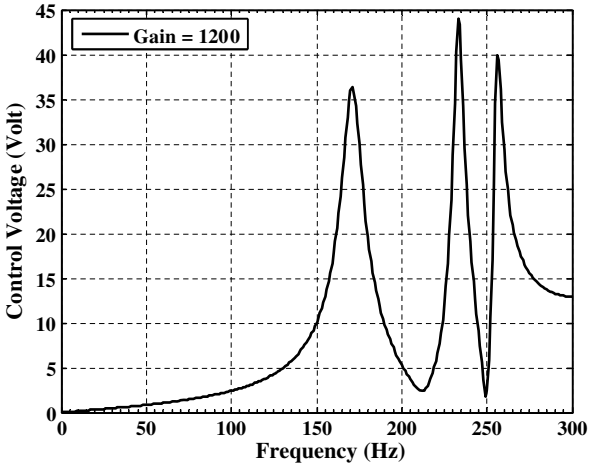

Fig. 4. Control voltage for the antisymmetric cross-ply (90°/0°) panel ($\phi = 30°$).

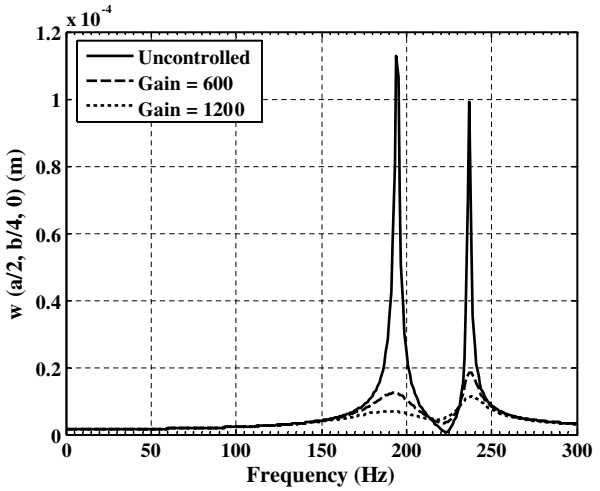

Fig. 5. Frequency response of an antisymmetric angle-ply (45°/−45°) panel ($\phi = 30°$).

Table 2
Amplitudes of the uncontrolled and controlled transverse displacement of the panels undergoing fundamental mode of vibration

Panel type	Control gain (K_d^j)	$w(a/2, b/4,0)$ (m)	Control voltage (V)
90°/0°	0	1.1484×10^{-4}	0
	600	0.4520×10^{-4}	29.14
	1200	0.2821×10^{-4}	36.38
45°/−45°	0	1.1268×10^{-4}	0
	600	0.1237×10^{-4}	9.18
	1200	0.0689×10^{-4}	12.25

gain increases, attenuation of the amplitudes of vibration also increases. The frequency response functions computed at the same point of a thin antisymmetric two layered angle-ply (−45°/45°) panel have been shown in Fig. 5. In this case also, the patches efficiently attenuate the amplitudes of vibrations enhancing the damping characteristics of the panel. For future reference, the magnitudes of the uncontrolled and controlled transverse

displacement of the panels subjected to active constrained layer damping and undergoing fundamental mode of vibration are presented in Table 2.

In order to investigate the effect of variation of fiber orientation (ψ) in the constraining PFRC layer of the patches on enhancing the damping characteristics of thin ($a/h = 100$) panels of different shallowness angles, the percentage attenuation of vibration of the panels are computed with different values of the piezoelectric fiber angle (ψ) using a particular value of control gain ($K_d^j = 600$) for both the patches. Percentage attenuation of the amplitude is determined with respect to the uncontrolled amplitude of vibration and may be an index for assessing the control authority of the patches. Only the fundamental mode $(1,1)$ of vibration has been targeted for investigating the attenuating capability of the patches. It has been reported elsewhere (Soldatos, 1983) that the cylindrical panel seems to show anomalous dynamic behavior for large values of shallowness angle. Hence, the variation of the values of the shallowness angle has been kept limited to 30° for investigating the effect of variation of piezoelectric fiber angle on the performance of the patches. Figs. 6 and 7 demonstrate

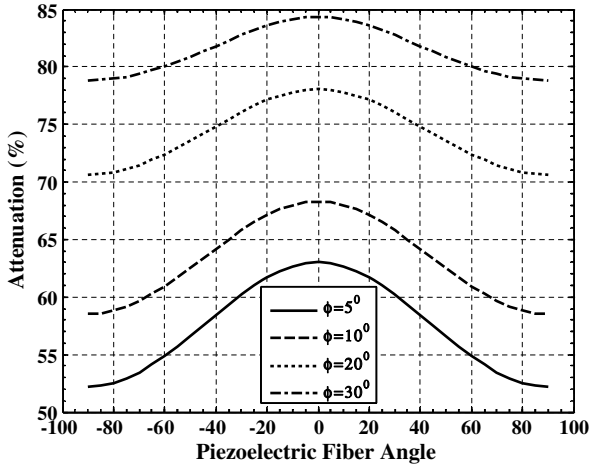

Fig. 6. Effect of fiber orientation (ψ) in the constraining PFRC layer and the shallowness angle (ϕ) on the control authority of the ACLD patches for controlling the first mode of vibration of a four layered antisymmetric cross-ply (0°/90°/0°/90°) panel.

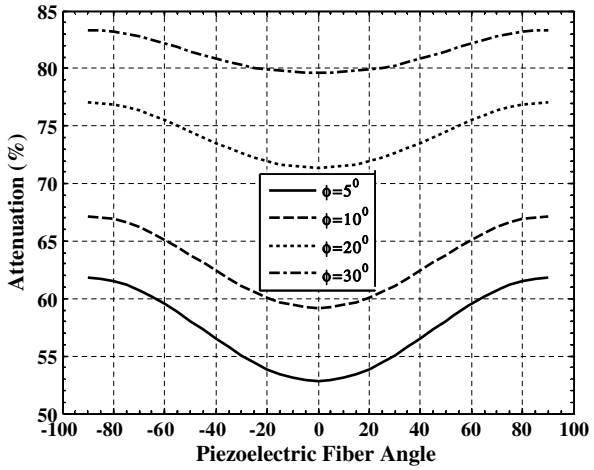

Fig. 7. Effect of fiber orientation (ψ) in the constraining PFRC layer and the shallowness angle (ϕ) on the control authority of the ACLD patches for controlling the first mode of vibration of a four layered antisymmetric cross-ply (90°/0°/90°/0°) panel.

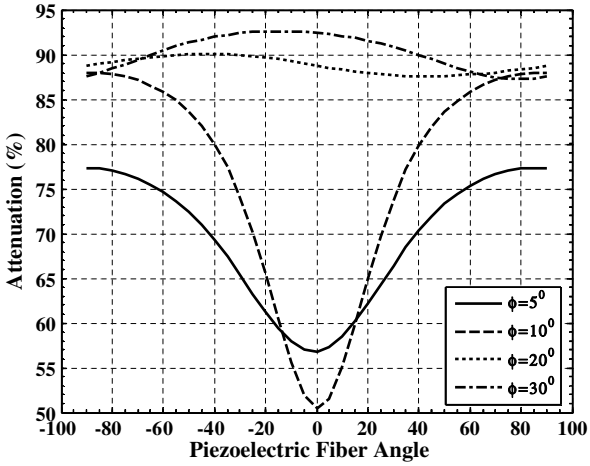

Fig. 8. Effect of fiber orientation in the constraining PFRC layer on the control authority of the ACLD patches for controlling the first mode of vibration of antisymmetric angle-ply panels ($-30°/30°/-30°/30°$).

the effect of variation of the piezoelectric fiber angle in the constraining PFRC layer on the control authority of the patches for different values of the shallowness angle of the antisymmetric cross-ply panels ($a/h = 100$ and $h = 0.004$ m). These results reveal that as the value of shallowness angle increases, the attenuating capability of the patches also increases irrespective of the cases where the fiber angle in the top layer of the panel is either 0° or 90°. It may also be observed from Figs. 7 and 8 that for different values of shallowness angle of the panel the optimum fiber angle in the PFRC layer is 0° or 90° according as the fiber orientation in the top layer of the substrate panel being integrated with the patches be 90° or 0°, respectively. Next, the effect of variation of fiber orientation in the constraining PFRC layer on the damping of first mode of vibration of antisymmetric angle-ply ($-\theta°/\theta°/-\theta°/\theta°/\ldots$) panels has been studied for different values of fiber angle (θ) in the orthotropic layers of the panels having different values of shallowness angle. Figs. 8–11 demonstrate this effect for the specific cases of four layered panels ($a/h = 100$ and $h = 0.004$ m) when the values of θ are considered as 30°, −30°, 45° and −45°, respectively. As shown in these figures, the plot for the attenuating capability of the patches for an angle-ply panel with lamination sequence ($-\theta°/\theta°/-\theta°/\theta°/././.$) is a mirror image of that for an angle-ply panel with lamination sequence ($\theta°/-\theta°/\theta°/-\theta°/././.$). That is, although the sign of the fiber angle (θ) in the orthotropic layers of the antisymmetric angle-ply substrate panels changes from positive to negative,

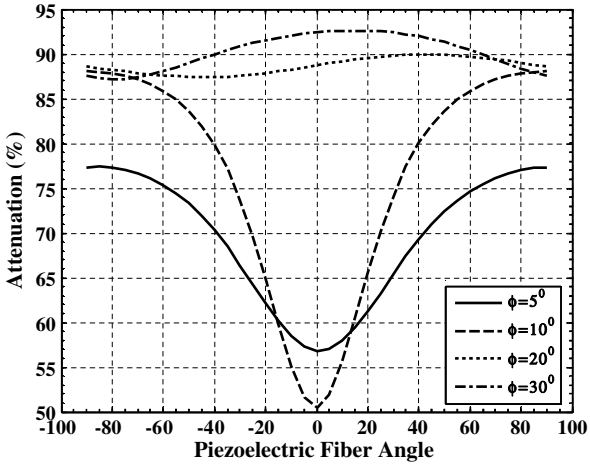

Fig. 9. Effect of fiber orientation in the constraining PFRC layer on the control authority of the ACLD patches for controlling the first mode of vibration of antisymmetric angle-ply panels ($30°/-30°/30°/-30°$).

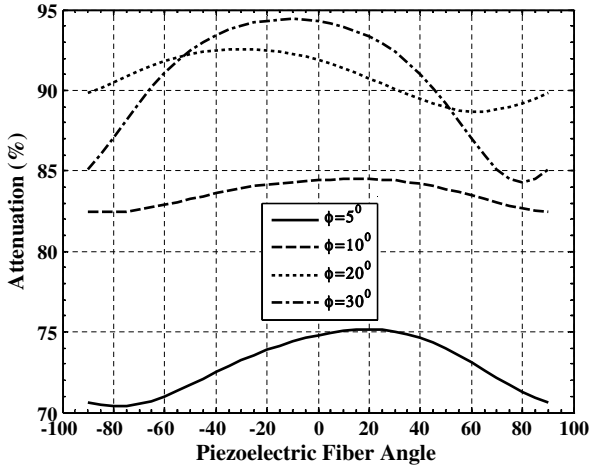

Fig. 10. Effect of fiber orientation (ψ) in the constraining PFRC layer and the shallowness angle (ϕ) on the control authority of the ACLD patches for controlling the first mode of vibration of a four layered antisymmetric angle-ply (−45°/45°/−45°/45°) panel.

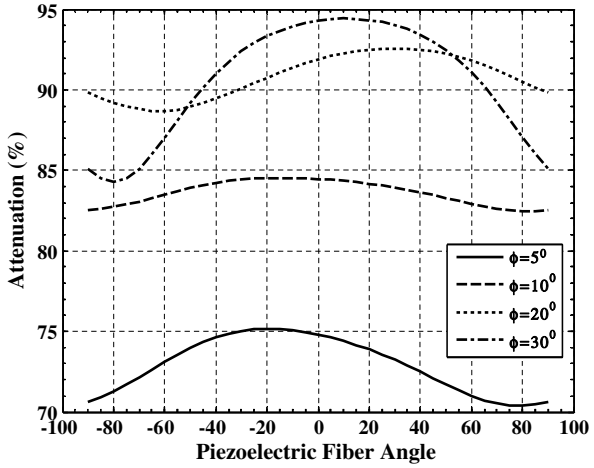

Fig. 11. Effect of fiber orientation (ψ) in the constraining PFRC layer and the shallowness angle (ϕ) on the control authority of the ACLD patches for controlling the first mode of vibration of a four layered antisymmetric angle-ply (45°/−45°/45°/−45°) panel.

the maximum attenuating capability of the patches remains same for a particular value of shallowness angle of the panels for controlling the first mode of vibration. However, the sign of the optimum value of the piezoelectric fiber angle becomes opposite. For example, in case of the angle-ply panel ($a/h = 100$ and $h = 0.004$ m) of lamination sequence (−30°/30°/−30°/30°) and 20° shallowness angle, the maximum attenuation is achieved when the value of the piezoelectric fiber angle (ψ) is −40° while the same is achieved for the angle-ply panel of lamination sequence (30°/−30°/30°/−30°) and 20° shallowness angle when the value of ψ is 40°. It may also be noted from Figs. 8–11 that the value of the piezoelectric fiber angle in the PFRC layer for attaining maximum damping of thin antisymmetric angle-ply panels varies with the different values of the shallowness angle and the attenuating capability of the patches also increases with the increase in the value of shallowness angle. The effect of number of layers in the panels of particular thickness on the performance of the patches has been demonstrated in Figs. 12 and 13 for thin antisymmetric cross-ply and angle-ply panels, respectively. As can be noticed from these figures, if the number of layers in the substrate panel is increased while the thickness of the panel remains constant, the maximum value of the attenuating capability of the patches marginally changes for both antisymmetric cross-ply and angle-ply panels.

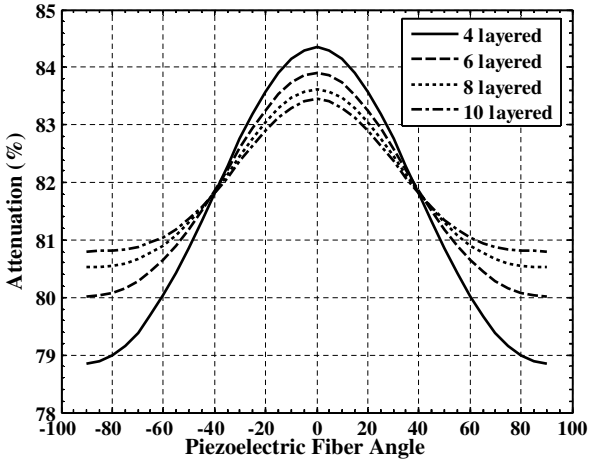

Fig. 12. Effect of fiber orientation (ψ) in the constraining PFRC layer and number of layers in the host panel on the control authority of the ACLD patches for controlling the first mode of vibration of a four layered antisymmetric cross-ply (0°/90°/0°/90°/./././.) panels ($\phi = 30°$).

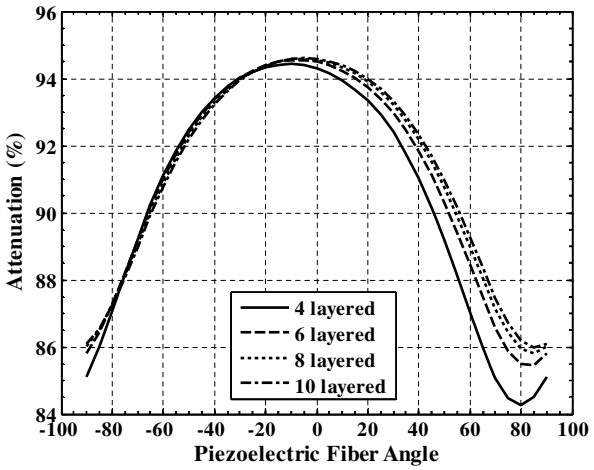

Fig. 13. Effect of fiber orientation (ψ) in the constraining PFRC layer and number of layers in the host panel on the control authority of the ACLD patches for controlling first mode of vibration of a four layered antisymmetric angle-ply (45°/−45°/45°/−45°/./././.) panels ($\phi = 30°$).

5. Conclusions

In this paper, a finite element analysis of active constrained layer damping (ACLD) of simply supported thin cylindrical laminated composite panels has been carried out to demonstrate the performance of the piezoelectric fiber reinforced composite (PFRC) materials as the material for the constraining layer of ACLD treatment. The finite element model is based on the first order shear deformation theories (FSDT). Antisymmetric cross-ply and angle-ply laminated composite panels are considered for evaluation of the numerical results. Two patches of ACLD treatment are used which are placed on the outer surface of the panels such that the fundamental modes are efficiently controlled. The results illustrate the significant enhancement of damping characteristics of the panels over the passive damping. The analysis revealed that the fiber orientation in the constraining PFRC layer of the ACLD patches and the shallowness angle of the panels play significant role in attenuating the vibration of thin laminated composite panels. In case of thin antisymmetric cross-ply panels, if the fiber angle in the orthotropic layer of the substrate panel being integrated with the patches be 0°

or 90° then the fiber angle in the constraining PFRC layer should be 90° or 0°, respectively to attain the maximum damping of first mode of vibration. For antisymmetric cross-ply panels, the control authority of the patches is independent of the sign of the piezoelectric fiber angle. In case of antisymmetric angle-ply panel $(-\theta^\circ/\theta^\circ/-\theta^\circ/\theta^\circ/\ldots)$ with a particular value of shallowness angle, the maximum value of the attenuating capability of the patches remains independent of the sign of the fiber angle (θ) in the orthotropic layer of the host panel being integrated with the patches. But the sign of the optimum fiber angle in the PFRC layer reverses when the fiber angle in the orthotropic layers of the panel changes its sign. For both antisymmetric cross-ply and angle-ply panels, the control authority of the patches increases with the increase in value of the shallowness angle. The optimum value of the piezoelectric fiber angle for maximum attenuation also varies with the different values of the shallowness angle of the antisymmetric angle-ply panels. Also, the performance of the patches is marginally affected when the number of orthotropic layers being present in the host panel increases.

The control of other higher modes requires the determination of optimal placement and number of the patches. Also, the investigation into the effect of other boundary conditions on the performance of the patches would be an important extension of this study. Thus several important and challenging researches may be pursued further following the work in this paper.

References

Agarwal, B.N., Treanor, K.E., 1999. Shape control of a beam using piezoelectric actuators. Smart Materials and Structures 8, 729–740.

Azvine, B., Tomlinson, G.R., Wynne, R.J., 1995. Use of active constrained layer damping for controlling resonant. Smart Materials and Structures 4, 1–6.

Badre-Alam, A., Wang, K.W., Gandhi, F., 1999. Optimization of enhanced active constrained layer treatment on helicopter flexbeams for aeromechanical stability augmentation. Smart Materials and Structures 8, 182–196.

Bailey, T., Hubbard, J.E., 1985. Distributed piezoelectric polymer active vibration control of a cantilever beam. Journal of Guidance Control and Dynamics 8 (5), 605–611.

Baz, A., Poh, S., 1988. Performance of an active control system with piezoelectric actuators. Journal of Sound and Vibration 126 (2), 327–343.

Baz, A., Poh, S., 1996. Optimal vibration control with modal positive position feedback. Optimal Control Applications and Methods 17, 141–149.

Baz, A., Ro, J., 1995. Optimum design and control of active constrained layer damping. ASME Journal of Vibrations and Acoustics 117B, 135–144.

Baz, A., Ro, J., 1996. Vibration control of plate with active constrained layer damping. Smart Materials and Structures 5, 272–280.

Chantalakhana, C., Stanway, R., 2001. Active constrained layer damping of clamped-clamped plate vibrations. Journal of Sound and Vibration 241 (5), 755–777.

Crawley, E.F., Luis, J.D., 1987. Use of piezoelectric actuators as elements of intelligent structures. AIAA Journal 25 (10), 1373–1385.

Devasia, S., Tesfay, M., Paden, B., Bayo, E., 1993. Piezoelectric actuator design for vibration suppression: placement and sizing. Journal of Guidance, Control and Dynamics 16, 859–864.

Dong, S., Tong, L., 2001. Vibration control of plates using discretely distributed piezoelectric quasi-modal actuators/sensors. AIAA Journal 39, 1766–1772.

Gu, Y., Clark, R.L., Fuller, C.R., 1994. Experiments on active control of plate vibration using piezoelectric actuators and polyvinylidyne fluoride (PVDF) modal sensors. ASME Journal of vibrations and acoustics 116, 303–308.

Hanagud, S., Obal, M.W., Calise, A.J., 1992. Optimal vibration control by the use of piezoceramic sensors and actuators. Journal of Guidance, Control and Dynamics 15 (5), 1199–1206.

Kapadia, R.K., Kawiecki, G., 1997. Experimental evaluation of segmented active constrained layer damping treatments. Journal of Intelligent Material Systems and Structures 8, 103–111.

Lee, C.K., Chiang, W.W., Sulivan, O., 1991. Piezoelectric modal sensor/actuator pairs for critical active damping vibration control. Journal of the Acoustical Society of America 90 (1), 374–384.

Liu, Y., Wang, K-W., 2002. Enhanced active constrained layer damping treatment for broadband vibration suppression. Journal of Vibration and Control 8, 777–803.

Mallik, N., Ray, M.C., 2003. Effective coefficients of piezoelectric fiber reinforced composites. AIAA Journal 41 (4), 704–710.

Peng, F., Ng, A., Hu, Y.R., 2005. Actuator placement optimization and adaptive vibration control of plate smart structure. Journal of Intelligent Material Systems and Structures 16, 263–271.

Plunkett, R., Lee, C.T., 1970. Length optimization for constrained viscoelastic layer damping. Journal of Acoustical Society of America 48, 150–161.

Ray, M.C., Mallik, N., 2004. Active control of laminated composite beams using a piezoelectric fiber reinforced composite layer. Smart Materials and Structures 13 (1), 146–152.

Ray, M.C., Mallik, N., 2004a. Finite element analysis of smart structures containing piezoelectric fiber reinforced composite actuator. AIAA Journal 42 (7), 1398–1405.

Ray, M.C., Mallik, N., 2005b. Performance of smart damping treatment using piezoelectric fiber reinforced composites. AIAA Journal 43 (1), 184–193.

Ray, M.C., Reddy, J.N., 2004. Optimal control of thin circular cylindrical panels using active constrained layer damping treatment. Smart Materials and Structures 13 (1), 64–72.

Ray, M.C., Reddy, J.N., 2005. Use of piezoelectric fiber reinforced composites for active control of laminated cylindrical composite shells. Composite Science and Technology 65 (7–8), 1226–1236.

Ray, M.C., Oh, J., Baz, A., 2001. Active constrained layer damping of thin cylindrical panels. Journal of Sound and Vibration 240 (5), 921–935.

Ro, J., Baz, A., 2002. Optimum placement and control of active constrained layer damping using modal strain energy approach. Journal of Vibration and Control 8, 861–876.

Shen, I.Y., 1996. Stability and controllability of Euler Bernoulli beams with intelligent constrained layer treatments. ASME Journal of Vibrations and Acoustics 118, 70–77.

Soldatos, K.P., 1983. Free vibrations of antisymmetric angle-ply laminated circular cylindrical panels. Quarterly Journal of Mechanics and Applied Mathematics 36 (2), 207–221.

Soldatos, K.P., 1984. A comparison of some shell theories used for the dynamic analysis of cross-ply laminated circular cylindrical panels. Journal of Sound and Vibration 97 (2), 305–319.

Stöbener, U., Gaul, L., 2000. Modal vibration control for PVDF coated plates. Journal of Intelligent Material Systems and Structures 11 (4), 283–293.

Sun, D., Tong, L., 2003. Effect of debonding in active constrained layer damping patches on hybrid control of smart beams. International Journal of Solids and Structures 40, 1633–1651.

Sung, Y., Kam, Y.S., 2000. A finite element formulation for composite laminates with smart constrained layer damping. Advances in Engineering Software 31, 529–537.

Tzou, H.S., Tseng, C.I., 1990. Distributed piezoelectric sensor/actuator design for dynamic measurement/control of distributed parameter systems: a piezoelectric finite element approach. Journal of Sound and Vibration 138 (1), 17–34.

Yau, D.T.W., Fung, E.H.K., 2005. Optimization of rotating flexible arm with ACLD treatment. Journal of Sound and Vibration 281, 1163–1174.

Zhou, R.C., Lai, Z., Xue, D.Y., Huang, J.K., Mei, C., 1995. Suppression of nonlinear panel flutter with piezoelectric actuators using finite element method. AIAA Journal 6, 1098–1105.